THERMAL MANAGEMENT OF A MULTI-FUNCTIONAL BATTERY CASE

İbrahim DİKER, idiker@cu.edu.tr Cukurova University, 01250, Adana, Türkiye

O. Cem GÖKCİLER, ocgokciler@cu.edu.tr Cukurova University, 01250, Adana, Türkiye

Göktürk M. ÖZKAN, gmozkan@cu.edu.tr Cukurova University, 01250, Adana, Türkiye

Durmuş Can ACER, dcacer@cu.edu.tr Cukurova University, 01250, Adana, Türkiye

Ahmet ÇETİN, acetin@adiyaman.edu.tr Adıyaman University, 02040, Adıyaman, Türkiye

Necdet GEREN, gerendr@cu.edu.tr Cukurova University, 01250, Adana, Türkiye

ABSTRACT

The current study aims to optimize the thermal management system of the composite battery case, which is planned to protect and improve the battery's safety and life cycle. The relatively heavier and more complex structure of liquid-cooled thermal management systems will be compensated by a composite battery case produced with a new patent-protected technique. The thermal management system will be studied first numerically to obtain an optimized geometry for the highest heat transfer and minimum pressure loss. Then, measurements will be performed on the manufactured battery case. Maximum surface temperature and pressure losses were compared according to the results of two different analyses with laminar and turbulent flow regimes.

Keywords: Liquid cooling battery thermal management system, Battery casing technology, Response surface methodology

ÖZET

Mevcut çalışma, batarya güvenliğini ve yaşam döngüsünü korumak ve iyileştirmek için planlanan kompozit batarya paketinin termal yönetim sistemini optimize etmeyi amaçlamaktadır. Sıvı soğutmalı termal yönetim sistemlerinin nispeten daha ağır ve karmaşık yapısı, yeni patent korumalı teknikle üretilen kompozit pil paketiyle telafi edilecek. Minimum basınç kaybı ile en yüksek ısı transferi için optimize edilmiş bir geometri elde etmek amacıyla termal yönetim sistemi ilk olarak sayısal olarak incelenecektir. Daha sonra üretilen batarya paketi üzerinde ölçümler yapılacaktır. Laminer ve türbülanslı akış rejimine sahip iki farklı analiz sonuçlarına göre maksimum yüzey sıcaklığı ve basınç kayıpları karşılaştırılmıştır.

Anahtar Kelime: Sıvı soğutmalı batarya termal yönetim sistemi, Batarya muhafaza teknolojisi, Yanıt yüzeyi yöntemi

1. INTRODUCTION

In recent years, the use of electric vehicles (EVs) and hybrid vehicles (HVs) is increasing rapidly [Yang et al. 2022]. The main reason for this uptrend is the environmental concerns such as; global warming and reducing air quality [Zhu et al. 2019]. EVs and HVs most commonly use lithium-ion (Li-ion) batteries because of their high energy density, long service life, reliability, and relatively wide operating temperature range [Senyshyn et al. 2015]. For the best performance, the Li-ion batteries should operate within the suggested operated temperature that has a range of 15 °C–35 °C [Pesaran et al. 2013]. Should the temperature of the batteries surpass this range, it could lead to safety hazards like fire or explosion. Additionally, beyond this temperature range, the efficiency, lifespan, and performance of the batteries decrease [Spitthoff et al. 2021]. Therefore, thermal management of the battery package of an EV/HV becomes an issue. The required thermal management is provided via thermal management systems that are attached to the battery packs. According to their heating/cooling mechanisms, thermal management systems have their advantages and disadvantages in battery packs, and they can be categorized into three distinct groups presented in Table 1 [Ali, 2023].

Various techniques aimed at dissipating heat from the battery pack or pre-heating/heating the batteries have been experimented with and tested by different research groups in recent years. The research that is performed by Mahamud et al. (2013) can be an example of the group of air cooling. Nevertheless, despite the simplicity of structure and lightweight, this approach is not as effective as liquid systems, as heat transfer is generally faster in liquids than in gases [Cengel, et al. 2015]. Thus, it is advisable to utilize liquid-based thermal management systems for more efficient heating/cooling of battery packs. The weight of the existing battery cooling systems is too heavy. A typical battery active cooling system consists of pipes, a water pump, a compressor, an evaporator, a condenser, and an expansion valve that creates additional weight [Kalaf et al. 2021].

The high efficiency of liquid-based thermal management systems has led to an increase in research activity in this area. As an example; A new direct liquid cooling strategy was suggested for large-scale lithium-ion pouch-type cells, aiming to maintain the cells' operating temperature within the optimal range for both performance and safety by Larranaga-Ezeiza

et al. (2022). As another example under this topic; He et al. (2023) designed a double-layered I-shaped liquid cooling plate to optimize the working temperature of a Li-ion battery.

Amongst studies on liquid-based thermal management systems, some focus specifically on the utilization of heating pipes to manage the temperature of the battery pack [Jaguemont and Van Mierlo, 2020]. Because of the benefits of liquid-based thermal management systems, leading companies such as Tesla and General Motors have incorporated these systems into their EVs [Kannan et al. 2021]. A typical liquid-to-liquid cooled active battery thermal management system schematic is shown in Figure 1 [Kalaf et al., 2021]. Although the advantages of liquid-based thermal management systems mentioned above are significant, it's important not to overlook some of their disadvantages. The existence of the piping system creates not only additional weight but also, manufacturing and maintenance costs [Khateeb et al., 2004]. Also, the failure possibility is increased due to the number of additional parts. To address the existing challenges of conventional thermal management systems, we propose a composite battery case with thermal management and self-healing capabilities, utilizing liquid thermal management as its foundation. The problem of the high weight can be overcome with a novel approach provided in this work. Because this battery casing does not contain any additional piping system, it is lighter. The liquid flow is facilitated through channels integrated within the composite layers, eliminating the need for additional piping materials. The thermal management channels are created within the Carbon Fiber Reinforced Polymer (CFRP) laminate by using a novel microvascular channel-creating method based on the patent-protected technique [Geren et al. 2024]. The required patent applications were made in 2022 and 2023 for this novel channel-creating method, for the name of Çukurova University. This approach makes the creation of the thermal management system cheaper, safer, and easier to apply.

Table 1. Comparison between different types of thermal management systems [Ali, 2023]

System Type	**Additional Thermal Power Source**	**Thermal Conductivity**	**Type of Thermal Management**	**System**	**Required Space**	**Cost**
Air Cooling	Exist	Low	Heating/Cooling	Basic	Large	Low
PCM	Non-exist	Low	Cooling	Basic	Small	Low
Liquid Cooling	Exist	High	Heating/Cooling	Complicated	Large	High

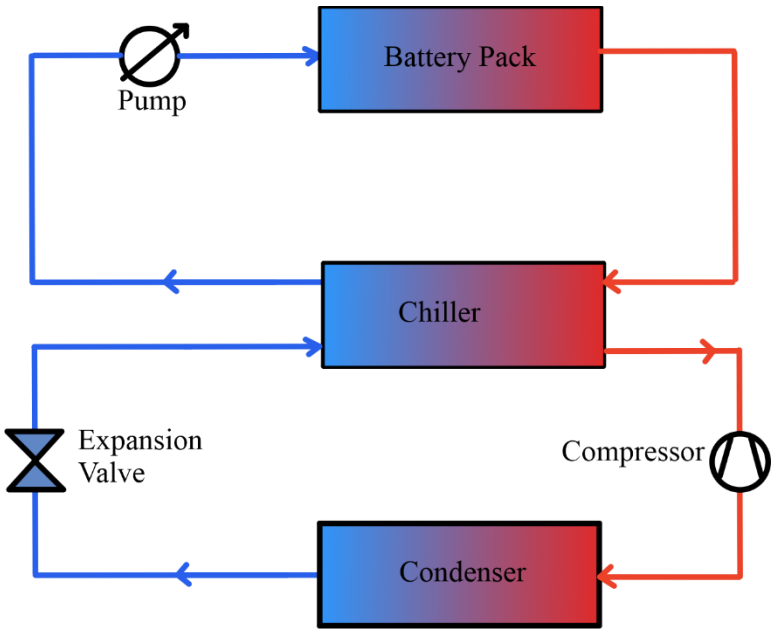


Figure 1. Schematic Representation of Liquid to Liquid Cooled Active Battery Thermal Management System

2. MATERIAL AND METHOD

In the current ongoing work of this project, the novel channel-creating method will be utilized to create the integrated channels with circular cross-section on the surface of the battery case (see in Figure 2). The channels will be located on the top and bottom surfaces of the battery case since the majority of the heat generated due to the internal resistance of battery cells originates from the top edges where connectors are located [Kim et al., 2009]. Four different independent parameters were determined to reduce the maximum surface temperature at the top of the battery pack. Hence the battery case and pack will be kept at an optimum operating temperature of the lithium-ion battery cells. In addition, the aim is also to minimize pressure losses through the piping system. Current work includes both experimental and numerical studies. First, the most suitable configuration for the thermal management system will be determined through numerical studies, and then the optimized configuration will be implemented based on the patent-protected technique [Geren et al. 2024] for experimental measurements.

An optimization study will be carried out to achieve this goal. The response surface methodology is selected for designing experiment runs and optimizing the parameters. Four independent and two dependent parameters are selected by taking into account the relevant studies, see Table 2 for the parameter details.

Table 2. Independent and Dependent Process Parameters

INDEPENDENT PARAMETERS	DEPENDENT PARAMETERS
Number Of Channels, n_c	Surface Temperature of Case, T
Temperature Of Inlet Flow, T_{in}	
Mass Flow Rate, $\dot{m}$	Pressure Loss Between Inlet and Outlet, ΔP
Heat Transfer Coefficient of The Case Material, k	

Response Surface Methodology (RSM) is a collection of statistical and mathematical techniques designed to optimize responses by analysing the independent and interactive effects of variables. RSM provides crucial information for experiments to determine model characteristics. The data generated from RSM are then used to develop a second-order predictive model that links input process parameters to response variables. In this study, the Box-Behnken Design (BBD) will be utilized, enabling the investigation of three input process parameters that influence responses with less time and fewer experimental runs compared to other experimental designs [Ozonoh et al. 2020].

The Bernardi equation (Equation 2.1) given below will be used to calculate the heat production in battery cells [Bernardi et al. 1985].

$$\dot{Q} = (V - V_{ADV})I + IT\frac{dV_{ADV}}{dT} \tag{2.1}$$

Where V is the cell voltage, V_{ADV} is the open circuit voltage, I is the current, and T is the cell temperature. The first term on the right side of the equation represents irreversible heat, while the second term is the reversible heat resulting from the change in entropy.

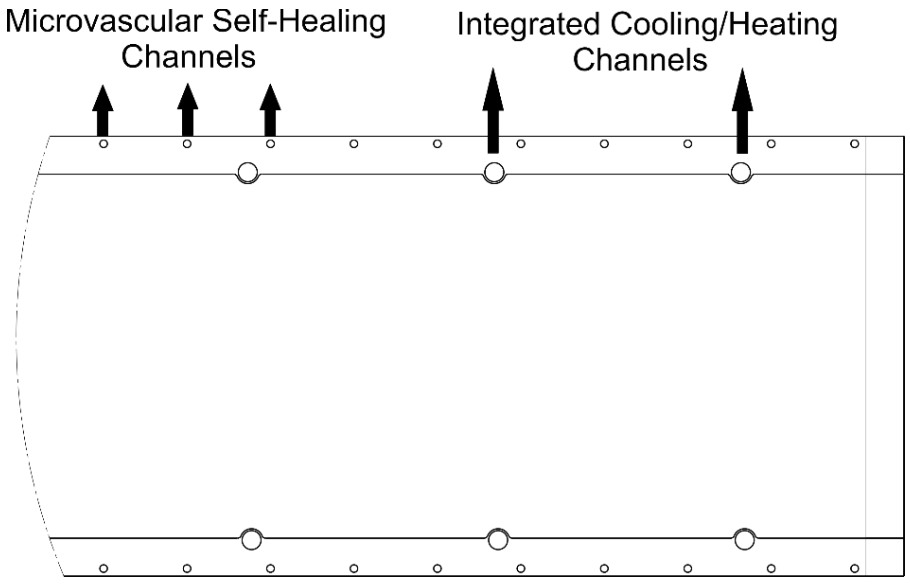


Figure 2. Schematic representation of microvascular self-healing and cooling/heating channels on top surface of battery package

The reversible heat in battery cells is much smaller compared to the irreversible heat, so it can be neglected [Qian et al., 2019]. In this case, equation 2.1 can be simplified as follows:

$$\dot{Q} = I^2 R \tag{2.2}$$

Where R indicates the internal resistance of the relevant battery cell. The cells to be included in the battery pack were chosen as "LG Chem E78" with an internal resistance of 1.48mΩ. With the 96S2P battery configuration obtained by connecting two of ninety-six serially connected battery cells in parallel, the total internal resistance was calculated as 71.04mΩ. The current passing through the battery pack was calculated as 72.3 Ω by dividing the power of the battery, which consumes 25 kW average power, by the nominal voltage value of 345.6V. According to Equation 2, the heat generated from the battery pack was calculated as 371W. When these obtained values are substituted in Equation 2.2, the battery heat released from the package can be calculated as Q̇=371W.

Heat transfer is divided into three groups: conduction, convection, and radiation. Radiative heat transfer in battery packs can be neglected because it is relatively low and difficult to simulate [Qian et al 2019; Zhao et al 2023]. Moreover, these assumptions must be made in order to perform the simulation [Chen et al 2006]: The thermal properties of the material do not change on the surfaces where heat transfer will take place, the specific heat capacity and thermal conductivity of the battery remain constant during charging and with temperature. Furthermore, these assumptions still need to be made: the thermal conductivity of the battery is anisotropic and the internal current is the average value, thus heat production is equal everywhere.

According to Fourier's law, conduction heat transfer occurs due to the internal temperature gradient and can be expressed as follows:

$$Q = -kA\frac{\partial T}{\partial x} \tag{2.3}$$

Where k, A and T are the heat conduction coefficient, surface area and temperature, respectively. The minus sign indicates that the direction of heat transfer is opposite to the temperature gradient. Convective heat transfer occurs between the battery cell at high temperature and the battery pack case at low temperature, thanks to natural convection, and can be expressed by the following equation:

$$Q = hA\Delta T \tag{2.4}$$

The h in the equation represents the convective heat transfer coefficient of the air inside the battery pack. The heat transfer equations in cartesian and cylindrical coordinates are given below with Equation 2.5 and 2.6, respectively:

$$\frac{\partial}{\partial x}\left(k\frac{\partial T}{\partial x}\right)+\frac{\partial}{\partial y}\left(k\frac{\partial T}{\partial y}\right)+\frac{\partial}{\partial z}\left(k\frac{\partial T}{\partial z}\right)+\dot{q}=\rho_c c_p\frac{\partial T}{\partial t} \tag{2.5}$$

$$\frac{1}{r}\frac{\partial}{\partial r}\left(kr\frac{\partial T}{\partial r}\right)+\frac{1}{r^2}\frac{\partial}{\partial \varphi}\left(k\frac{\partial T}{\partial \varphi}\right)+\frac{\partial}{\partial z}\left(k\frac{\partial T}{\partial z}\right)+\dot{q}=\rho c_p\frac{\partial T}{\partial t} \tag{2.6}$$

Where ρ_c, c_p, and $\dot{q}$ express body density, specific heat at constant pressure and volumetric heat flow, respectively.

ANSYS FLUENT 20.0, a computational fluid dynamics commercial package program, will be used to simulate the flow characteristics and thermal behavior. Differences in thermal behavior with laminar and turbulent flow structures with different Reynolds numbers (Re) will be examined. Moreover, the effect of the channel geometry and configuration through which the refrigerant passes on heat transfer will be revealed. The governing equations given below, continuity, momentum, energy, k, and ε respectively, will be discretized by the finite volume method.

$$\frac{\partial \rho}{\partial t}+\nabla\cdot(\rho u)=0 \tag{2.7}$$

where ρ is density, u is mean velocity, t is the time.

$$\frac{\partial(\rho u)}{\partial t}+\nabla\cdot(\rho u u)=-\nabla p+\nabla\cdot(\mu\nabla u)+f \tag{2.8}$$

where p is the pressure, μ is viscosity, f is the body forces.

$$\frac{\partial(\rho E)}{\partial t}+\nabla\cdot(\rho u E)=-\nabla\cdot(up)+\nabla\cdot(\kappa\nabla T)+\Phi \tag{2.9}$$

where E is the total energy (internal and kinetic), T is the temperature, κ is thermal conductivity, Φ is the work done by viscosity.

$$\frac{\partial(\rho k)}{\partial t}+\nabla\cdot(\rho \boldsymbol{u} k)=\nabla\cdot\left[\left(\mu+\frac{\mu_t}{\sigma_k}\right)\nabla k\right]+P_k-\rho\epsilon \tag{2.10}$$

$$\frac{\partial(\rho \epsilon)}{\partial t}+\nabla\cdot(\rho \boldsymbol{u} \epsilon)=\nabla\cdot\left[\left(\mu+\frac{\mu_t}{\sigma_\epsilon}\right)\nabla \epsilon\right]+C_{\epsilon 1}\frac{\epsilon}{k}P_k-C_{\epsilon 2}\epsilon \tag{2.11}$$

Where k is turbulent kinetic energy, ε is dissipation rate, P_k is the turbulent kinetic energy production, μ_t is turbulent viscosity, σ_k and σ_ϵ are Prandtl numbers, and $C_{\epsilon 1}$and $C_{\epsilon 2}$ are model constants.

Details about the CFD analysis setup settings are given in Table 3.

Table 3. CFD Analysis Setup Settings in Ansys Fluent

Solver Type	• Pressure-based
Time Stepping	• Steady
Pressure-Velocity Coupling	• Coupled
Viscous Model	• Laminar and Standard k-epsilon with Standard Wall Function
Energy Equation	• On
Fluid Properties	• Water • Density 1000 kg/m^3 • Dynamic viscosity 0.001 kg/ms • Thermal conductivity 0.6 w/mK • Specific Heat 4182 J/kgK
Solid Properties	• Carbon Fiber Reinforced Polymer • Density 1750 kg/m^3 • Specific Heat 750 J/kgK • Thermal Conductivity 0.7w/mK
Boundary Condition	• Inlet and Outlet mass flow rates are 0.0059 and 0.0196 kg/s. • Reynolds Numbers are 1500 and 5000 • Inlet flow temperature 10°C
Residual Monitors	• Residuals were set to be 1e-06
Initialization	• Standard Initialization

The grid structure utilized in the numerical analysis for our ongoing project is illustrated in Figure 3. The average orthogonal quality and skewness values of the grid structure, which consists of a total of 36.4 million elements, are 0.76 and 0.23, respectively.

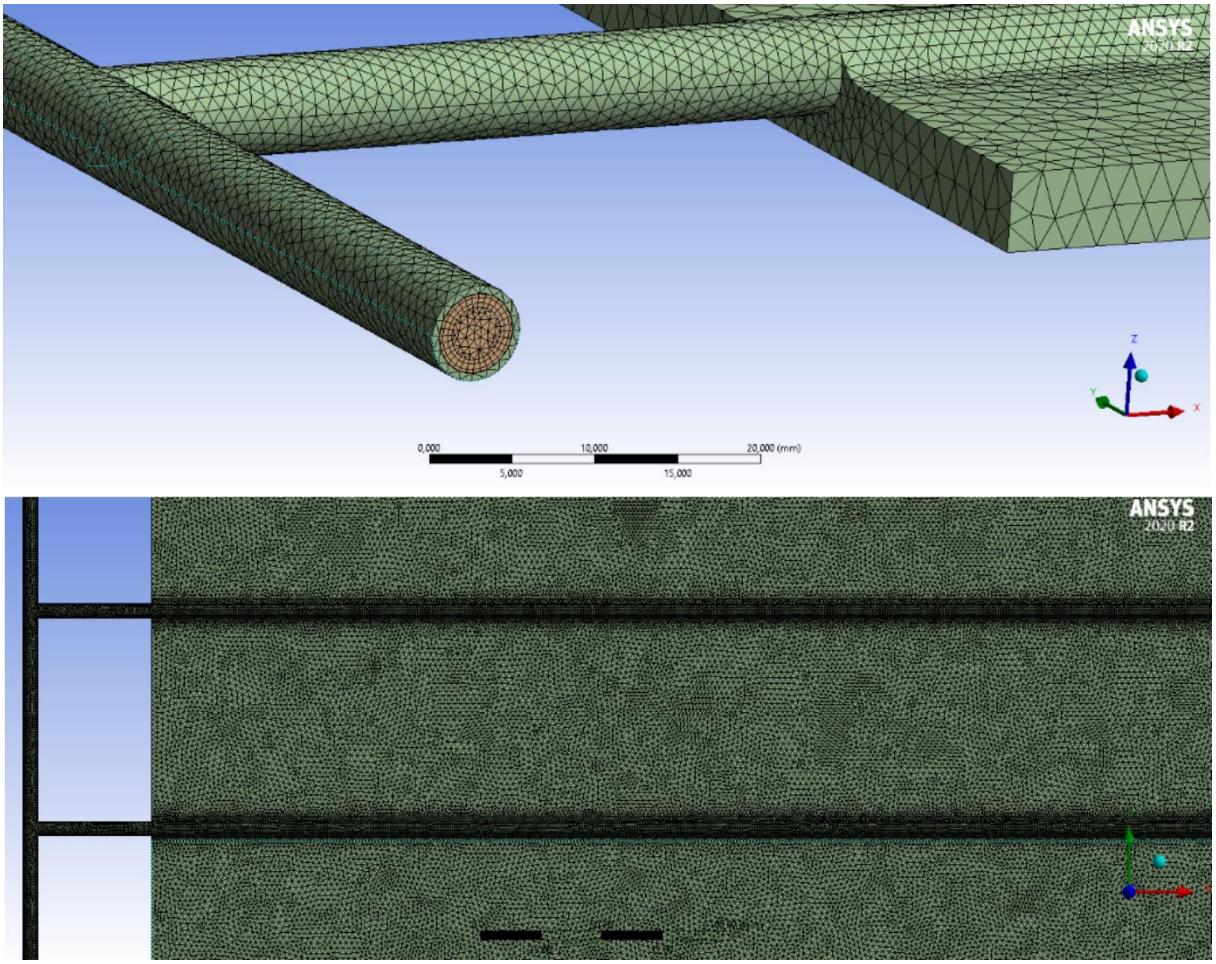


Figure 3. Grid Structure of Battery Case Surface

Flow domain and boundary conditions are defined in Figure 6.

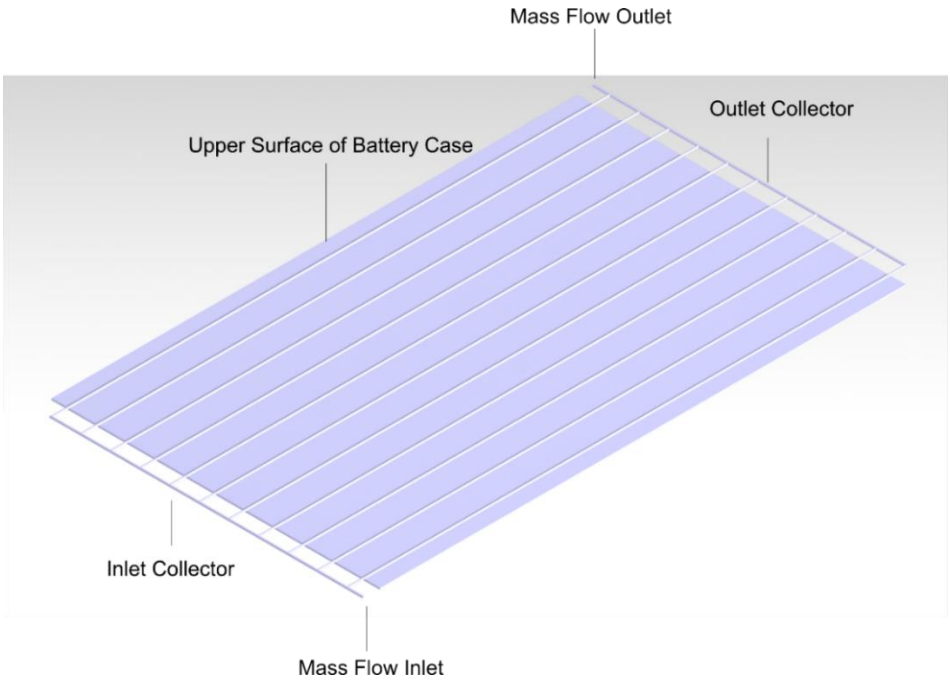


Figure 6. Solid model of the cooling/heating surface of the battery case

3. Preliminary Numerical Analyses

In the CFD model, the Coupled solver scheme was utilized which involves simultaneous solution of momentum continuity and energy equations, ensuring tighter coupling between velocity and pressure fields compared to the other schemes. The standard k-ε model was employed to simulate turbulent fluid flow. In order to obtain more accurate results, the convergence criteria of residuals have been set to 10^{-6}. Initially, the upper cover of the battery case with 11 cooling/heating channels with a heat transfer coefficient of 0.7W/mK was considered, and laminar and turbulent flow regimes were solved. The inlet water temperature was selected as 10 °C and the mass flow rate was determined as 0.0059 and 0.0196 kg/s for laminar and turbulent flow, respectively.

Grid independence analysis was performed to ensure that the analyses performed and to be performed are independent of the grid structure. In Figure 4, the pressure loss differences between the inlet and outlet with five different element numbers are examined.

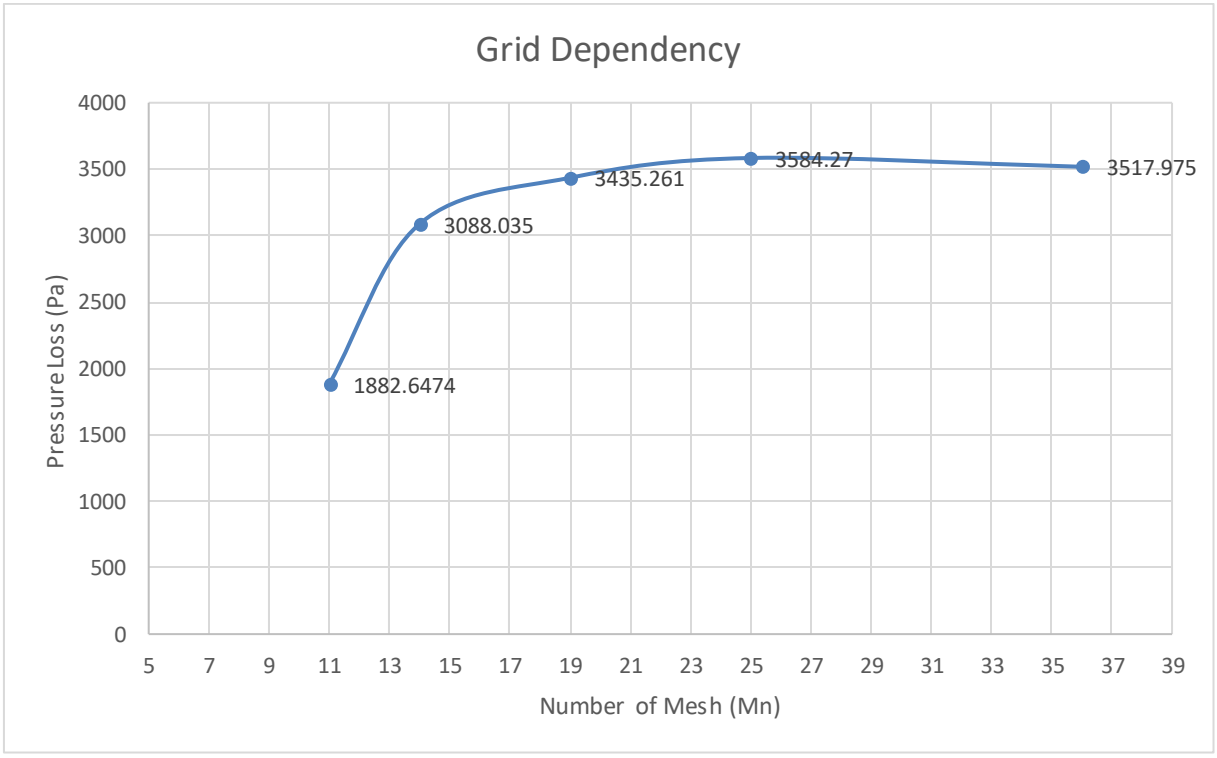
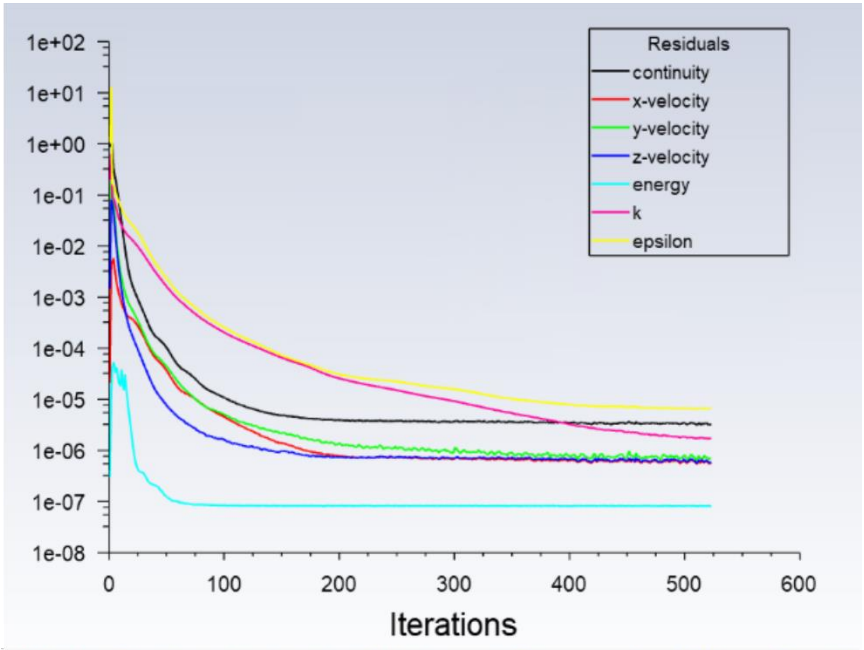


Figure 4. Graph of Grid Dependency Analysis

The residual graph of the numerical analyses performed in Ansys Fluent is presented in Figure 5 to show that the results converge.



iter	continuity	x-velocity	y-velocity	z-velocity	energy	k	epsilon	time/iter	
518	3.3825e-06	6.0212e-07	7.5698e-07	6.2930e-07	8.1761e-08	1.7378e-06	6.5541e-06	3:26:09	246
519	3.4464e-06	6.1672e-07	7.1463e-07	6.4225e-07	8.1969e-08	1.7078e-06	6.5005e-06	3:25:54	245
520	3.2690e-06	5.6852e-07	7.3878e-07	6.1036e-07	8.2284e-08	1.7303e-06	6.5983e-06	3:23:54	244
521	3.1623e-06	5.6101e-07	6.5859e-07	5.9106e-07	8.2295e-08	1.7125e-06	6.6012e-06	3:23:46	243
522	3.2240e-06	5.5851e-07	7.0936e-07	5.7961e-07	8.1733e-08	1.7272e-06	6.5734e-06	3:23:29	242
523	3.2330e-06	5.6261e-07	7.0802e-07	5.6962e-07	8.1276e-08	1.7270e-06	6.6277e-06	3:27:06	241
524	3.4295e-06	6.1463e-07	8.0038e-07	6.5272e-07	8.2117e-08	1.7448e-06	6.6814e-06	3:32:11	240

Done.

Figure 5. Graph of Residual Monitor

Figure 7 shows the temperature and pressure contours for the laminar flow regime at Re=1500. According to the results, the maximum temperature is found to be 105 °C near the exit of channels around the center of plate. Such a temperature is at a level that may degrade the structure of the composite material's resin. Furthermore, the temperature distribution across the plate is highly non-uniform which can damage the battery cell at the down region of the outlet side. Therefore, a laminar flow regime is found to be unsafe for battery life.

The effects of turbulent flow at a Reynolds Number on both heat transfer and pressure loss are illustrated in Figure 8. This figure demonstrates how the presence of turbulence enhances the convective heat transfer as a result of intensified mixing and fluid movement. Additionally, it highlights the corresponding increase in pressure drop, which is a consequence of the higher frictional forces encountered within the turbulent regime. Firstly, much more uniform temperature distribution is obtained on the plate compared to the laminar flow case (Figure 7). Moreover, the maximum surface temperature is decreased to 92 °C at the side regions of the plate, indicating high heat transfer around the channels. However, pressure loss between the inlet and outlet is increased from ΔP=455 Pa to ΔP=3517 Pa

when compared to the laminar flow case. In conclusion, the preliminary numerical analysis showed the favorable and unfavorable characteristics of laminar and turbulent flows i.e. laminar flow provides lower pressure loss but non-uniform temperature distribution through the plate whereas the reverse situation is true for the turbulent flow conditions. The preliminary study results of the cooling and heating system that we will use in our ongoing project coincide with the results of studies with similar configurations in the literature [Fan et al., 2023]. Therefore, more analyses are planned to obtain an optimized case giving the best configuration of channels on the plate. Hence, the upcoming numerical analysis will involve the prescribed independent parameters which are the number of channels (n_c), mass flow rate ($\dot{m}$), inlet water temperature (T_{in}), and heat conduction coefficient (k) to obtain the lowest surface temperature distribution by minimizing the pressure loss.

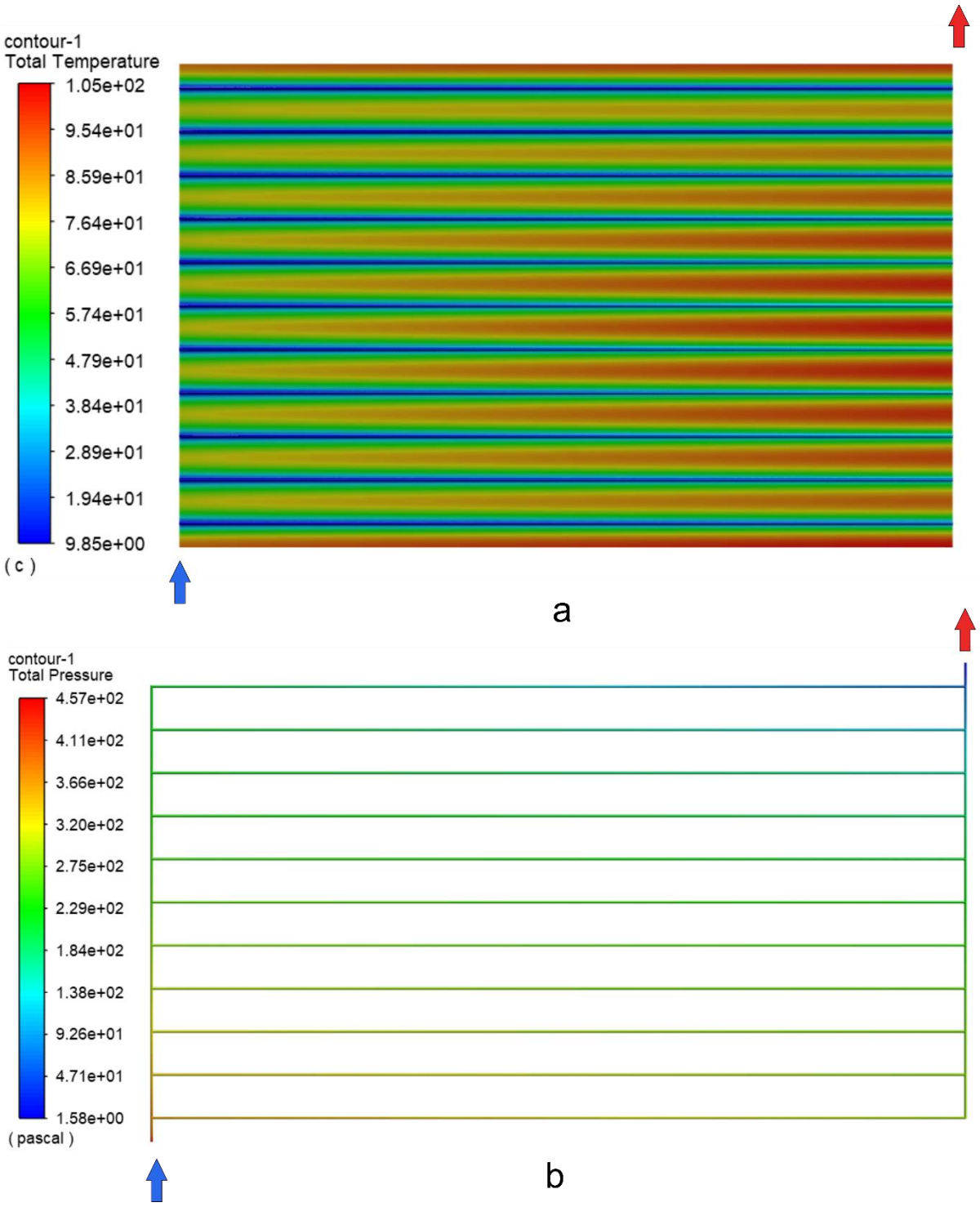


Figure 6. Temperature and Pressure Contours at Re=1500

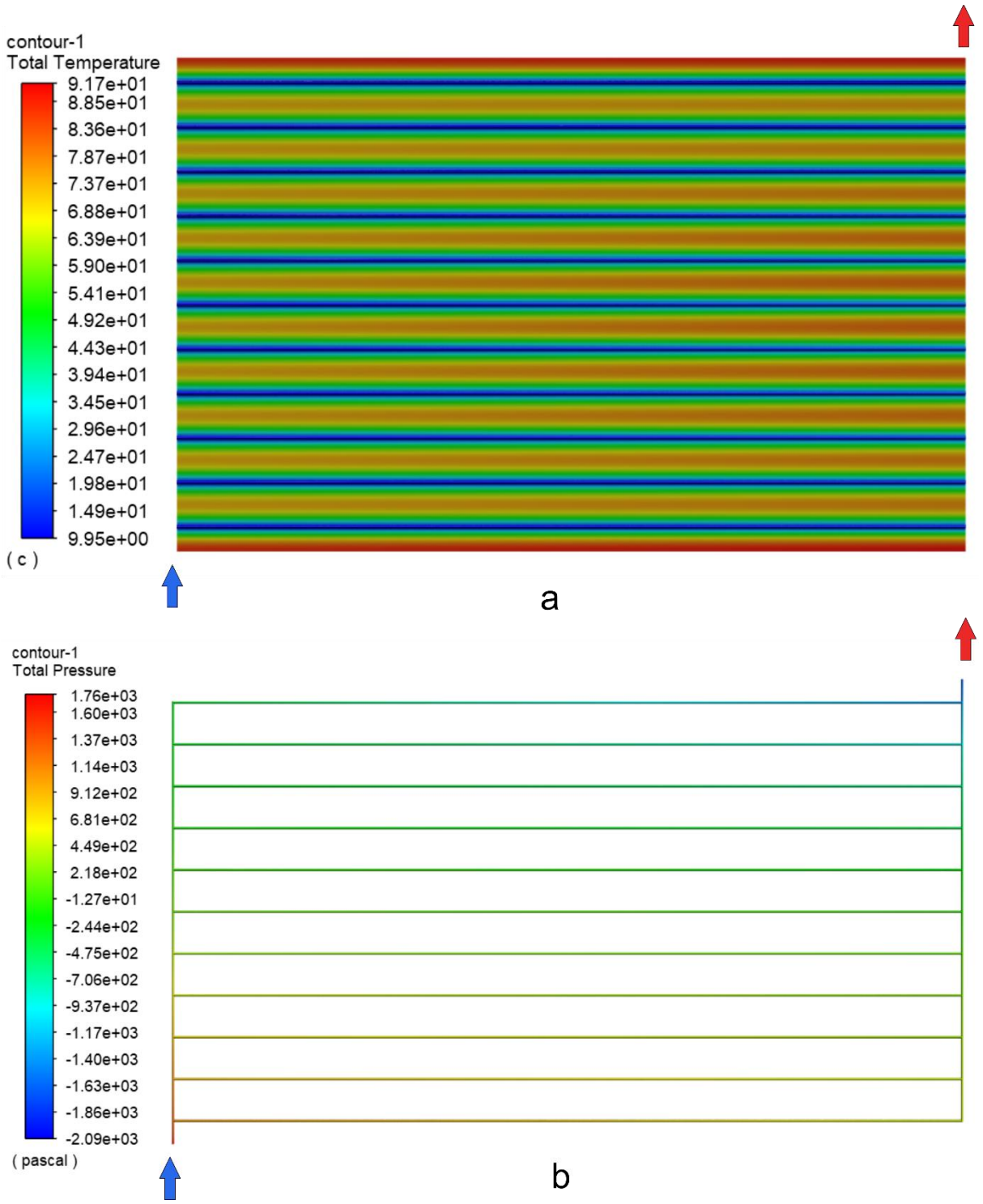


Figure 7. Temperature and Pressure Contour at Re=5000

4. CONCLUSION

In this paper, the thermal optimization characteristics of a novel battery case that has a thermal management system integrated within the CFRP. The required thermal analysis for this patent-protected project [Geren et al., 2024] is performed and proposed in this paper. Initially, the thermal management system will undergo numerical investigation to derive an optimized geometry that maximizes heat transfer while ensuring uniform temperature distribution and minimal pressure loss. After this numerical approach, measurements will be performed on the manufactured battery case.

To sum up, the initial numerical analysis revealed both advantageous and disadvantageous aspects of laminar and turbulent flows. For instance, laminar flow exhibits reduced pressure loss but results in non-uniform temperature distribution across the plate, whereas turbulent flow conditions present the opposite scenario. Consequently, further analyses are scheduled to achieve an optimized scenario determining the ideal configuration of pipes on the plate. Subsequently, the forthcoming numerical analysis will incorporate predetermined independent parameters: the number of pipes (np), mass flow rate ($\dot{m}$), inlet water temperature (Tin), and heat conduction coefficient (k), aiming to minimize pressure loss and achieve the most uniform surface temperature distribution. The preliminary numerical analysis of the thermal management system of this ongoing work is presented in this study. According to the analyses shown in the results section, independence from the number of grids and convergence of iterations, low pressure loss was achieved in the laminar flow regime, while low surface temperature was obtained in the turbulent flow regime.

ACKNOWLEDGEMENTS

The study was supported by the Scientific Research Projects Coordination Unit (BAP) of Cukurova University in Adana, Turkey, under grant No: FBA-2024-16561. Also, this project is supported by ‘Support Programme of Research Universities’ (ADEP).

REFERENCES

1. **Yang, Z., Li, Q., Yan, Y., Shang, W.-L., & Ochieng, W. (2022).** Examining influence factors of Chinese electric vehicle market demand based on online reviews under moderating effect of subsidy policy. Applied Energy, Vol.326, pp 120019.

2. **Zhu, X., Ren, M., Wu, G., Pei, J., & Pardalos, P. M. (2019).** Promoting new energy vehicles consumption: The effect of implementing carbon regulation on automobile industry in China. Computers & Industrial Engineering, Vol.135, pp 211–226.
3. **Senyshyn, A., Mühlbauer, M. J., Dolotko, O., & Ehrenberg, H. (2015).** Low-temperature performance of Li-Ion Batteries: The behavior of lithiated graphite. Journal of Power Sources, Vol.282, pp 235–240.
4. **Pesaran, A., S. Santhanagopalan and G. Kim (2013),** Addressing the impact of temperature extremes on large format li-ion batteries for vehicle applications (presentation), National Renewable Energy Lab.(NREL), Golden, CO (United States).
5. **Spitthoff, L., P. R. Shearing and O. S. Burheim (2021),** "Temperature, ageing and thermal management of lithium-ion batteries." Energies Vol.14, No.5, pp 1248.
6. **Ali, H. M. (2023),** "Thermal management systems for batteries in electric vehicles: A recent review." Energy Reports, Vol.9, pp 5545-5564.
7. **Mahamud, R. and C. Park (2011),** "Reciprocating air flow for Li-ion battery thermal management to improve temperature uniformity." Journal of Power Sources Vol.196, No.13, pp 5685-5696.
8. **Cengel, Y. A., A. J. Ghajar and M. Kanoglu (2015),** "Heat and mass transfer: fundamentals and applications
9. **Kalaf, O., D. Solyali, M. Asmael, Q. Zeeshan, B. Safaei and A. Askir (2021),** "Experimental and simulation study of liquid coolant battery thermal management system for electric vehicles: A review." International journal of energy research 45(5): 6495-6517.
10. **Larrañaga-Ezeiza, M., G. Vertiz, P. Arroiabe, M. Martinez-Agirre and J. Berasategi (2022),** "A novel direct liquid cooling strategy for electric vehicles focused on pouch type battery cells." Applied Thermal Engineering 216: 118869.
11. **He, P., H. Lu, Y. Fan, H. Ruan, C. Wang and Y. Zhu (2023),** "Numerical investigation on a lithium-ion battery thermal management system utilizing a double-layered I-shaped channel liquid cooling plate exchanger." International Journal of Thermal Sciences 187: 108200.
12. **Jaguemont, J. and J. Van Mierlo (2020),** "A comprehensive review of future thermal management systems for battery-electrified vehicles." Journal of Energy Storage 31: 101551.

13. **Kannan, C., Vignesh, R., Karthick, C., and Ashok, B., (2021),** "Critical review towards thermal management systems of lithium-ion batteries in electric vehicle with its electronic control unit and assessment tools." Proceedings of the Institution of Mechanical Engineers, Part D: Journal of Automobile Engineering 235(7): 1783-1807

14. **Khateeb, S. A., Farid, M. M., Selman, J. R., & Al-Hallaj, S. (2004).** Design and simulation of a lithium-ion battery with a phase change material thermal management system for an electric scooter. Journal of Power Sources, Vol.128(2), pp 292–307.

15. **Geren, N., Kostur, E.** Patent Title: Weaving threads forming microvascular channels into fibers in the production of fiber-reinforced polymer composites (Buluş başlığı: fiber takviyeli polimer kompozit üretiminde mikrovasküler kanal oluşturan ipliklerin elyaf içine dokunması), Application Number: PCT/TR2023 051362, Applicants: Cukurova University.

16. **Kim, U. S., Shin, C. B., & Kim, C.-S. (2009),** Modeling for the scale-up of a lithium-ion polymer battery. Journal of Power Sources, 189(1), 841–846.

17. **Ozonoh, M., Oboirien, B. O., & Daramola, M. O. (2020),** Optimization of process variables during torrefaction of coal/biomass/waste tyre blends: Application of Artificial Neural Network & Response Surface Methodology. Biomass and Bioenergy, 143, 105808.

18. **Bernardi, D., Pawlikowski, E., & Newman, J. (1985),** A general energy balance for battery systems. Journal of The Electrochemical Society, 132(1), 5–12.

19. **Qian, X., Xuan, D., Zhao, X., & Shi, Z. (2019),** Heat dissipation optimization of lithium-ion battery pack based on Neural Networks. Applied Thermal Engineering, 162, 114289.

20. **Zhao, L., Li, W., Wang, G., Cheng, W., & Chen, M. (2023),** A novel thermal management system for lithium-ion battery modules combining direct liquid-cooling with forced air-cooling. Applied Thermal Engineering, 232, 120992.

21. **Chen, S.-C., Wang, Y.-Y., & Wan, C.-C. (2006),** Thermal analysis of spirally wound lithium batteries. Journal of The Electrochemical Society, 153(4).

22. **Fan, X., Meng, C., Yang, Y., Lin, J., Li, W., Zhao, Y., Xie, S., & Jiang, C. (2023).** Numerical optimization of the cooling effect of a bionic fishbone channel Liquid Cooling Plate for a large prismatic lithium-ion battery pack with high discharge rate. Journal of Energy Storage, Vol.72, pp 108239.